Radiative forcing from halogen reservoir and halocarbon breakdown products

Thornhill, G. D. ORCID: https://orcid.org/0000-0002-6406-1414, Smith, L. A. and Shine, K. P. ORCID: https://orcid.org/0000-0003-2672-9978 (2024) Radiative forcing from halogen reservoir and halocarbon breakdown products. Journal of Geophysical Research: Atmospheres, 129 (12). e2024JD040912. ISSN 2169-8996 doi: 10.1029/2024JD040912 Available at https://centaur.reading.ac.uk/116851/

JGR Atmospheres

RESEARCH ARTICLE
10.1029/2024JD040912

Radiative Forcing From Halogen Reservoir and Halocarbon Breakdown Products

Gillian D. Thornhill[1], **Lucy A. Smith**[1], **and Keith P. Shine**[1]

[1]Department of Meteorology, University of Reading, Reading, UK

Key Points:

- Radiative forcing (RF) from four halogen reservoir or halocarbon breakdown species are quantified using satellite-derived distributions
- The total global-mean stratospherically-adjusted RF is estimated to be about 7 mW m^{-2} since about 1940
- This enhances the best estimate of the total halocarbon RF (including indirect effects) by about 3%

Supporting Information:

Supporting Information may be found in the online version of this article.

Correspondence to:

K. P. Shine,
k.p.shine@reading.ac.uk

Citation:

Thornhill, G. D., Smith, L. A., & Shine, K. P. (2024). Radiative forcing from halogen reservoir and halocarbon breakdown products. *Journal of Geophysical Research: Atmospheres*, *129*, e2024JD040912. https://doi.org/10.1029/2024JD040912

Received 30 JAN 2024
Accepted 8 JUN 2024

Author Contributions:

Conceptualization: Keith P. Shine
Formal analysis: Gillian D. Thornhill, Lucy A. Smith, Keith P. Shine
Funding acquisition: Keith P. Shine
Investigation: Gillian D. Thornhill, Lucy A. Smith, Keith P. Shine
Methodology: Gillian D. Thornhill, Lucy A. Smith, Keith P. Shine
Project administration: Keith P. Shine
Software: Gillian D. Thornhill, Keith P. Shine
Supervision: Keith P. Shine
Visualization: Gillian D. Thornhill
Writing – original draft: Gillian D. Thornhill, Keith P. Shine
Writing – review & editing: Gillian D. Thornhill, Lucy A. Smith, Keith P. Shine

Abstract The direct radiative forcing (RF) from halocarbons is reasonably well characterized. However, the forcing due to polyatomic halogen reservoir and halocarbon breakdown products has not previously been quantified and it is important to estimate this contribution. Four gases, $ClONO_2$, $COCl_2$, COF_2 and COClF, are considered; their stratospheric abundances mostly originate from the breakdown of chlorofluorocarbons, hydrochlorofluorocarbons and CCl_4. They have significant mid-infrared absorption bands and peak stratospheric mole fractions ranging from around 20 ppt to over 1 ppb, which are large compared to typical abundances of many emitted halocarbons. Using satellite observations of stratospheric abundance, observed infrared spectra, and a narrow-band radiation code, the stratosphere-adjusted radiative forcings (SARF) is computed. The global-annual mean SARF is estimated to be 7 ± 0.8 mW m^{-2} based on measured abundances in the period 2004–2019, with $ClONO_2$ contributing about 50%. Whilst not a major contributor to anthropogenic RF, only six individual halocarbon gases cause a significantly greater forcing. This forcing is then approximately attributed to their source gases; for most, it modestly enhances (by 1%–3%) both their direct RF and their global warming potentials. The most significant enhancement (5%–15%) is to CCl_4, the principal source of stratospheric $COCl_2$ and contributor to $ClONO_2$ abundances; disagreement in recent satellite-based $COCl_2$ retrievals is a significant source of uncertainty. These additional gases enhance the available best estimate of the total forcing due to halocarbon source gases (including e.g., ozone depletion) by about 3%; notably, this is the only identified indirect mechanism that increases, rather than decreases, total halocarbon forcing.

Plain Language Summary Halocarbon gases are widely used (e.g., in refrigeration and air conditioning). Any leakage to the atmosphere can contribute to environmental impacts, including ozone depletion and climate change. These contributions are reasonably well understood. This paper focuses on a previously neglected area. Once in the atmosphere, these gases break down into other gases, the abundances of which are available from satellite observations. These observations, and laboratory measurements of their infrared absorption properties, are used here to calculate the climate impact of four such gases for the first time. Their collective effect is relatively modest but only six individual halocarbons of the many emitted by human activity have a clearly larger effect. The total climate effect of emitted halocarbons includes their impact on stratospheric ozone depletion; when this is accounted for, these newly considered gases contribute about 3% to this total. For individual emitted halocarbons, the relative effect of these breakdown products can be larger, most notably for carbon tetrachloride, a gas previously used as a solvent, but now used as a feedstock for production of non-ozone-depleting halocarbons. These new results will contribute to assessments of the total climate effects of emitted halocarbons and the climate impact of legislation aimed at reducing emissions.

1. Introduction

The contribution of halocarbons to anthropogenic radiative forcing (RF) and climate change is well documented (e.g., Forster et al., 2021; Hodnebrog et al., 2020). In the most recent Intergovernmental Panel on Climate Change (IPCC) assessment (Forster et al., 2021), the 1750–2019 effective RF due to the direct effect of halogenated species was given as 0.41 W m^{-2}, with almost all of it occurring since 1940; this is 13% of the total well-mixed greenhouse gas forcing, and leads to an estimated warming (1750–2019) of about 0.2°C.

The full climate impact of halocarbons depends also on indirect effects, including ozone depletion (e.g., Szopa et al., 2021; WMO, 2022). Many molecules resulting from the breakdown of halocarbons (e.g., Burkholder et al., 2015) might also act as significant greenhouse gases; this has not previously been considered, beyond simplified calculations assuming such gases to be well mixed. The focushere is on 4 polyatomic molecules that

have significant vibrational-rotational absorption bands in the mid-infrared, and which arepresent in the stratosphere at concentrations significant compared to those of the parent halocarbons. In the terminology of Burkholder et al. (2015) three are "first generation major degradation products", carbonyl fluoride (COF_2), phosgene ($COCl_2$) and carbonyl chlorofluoride (COClF); the fourth, chlorine nitrate ($ClONO_2$), is a major reservoir species of reactive chlorine.

The questions we seek to answer are whether collectively these gases contribute significant RF, and whether this RF significantly changes the RF that can be attributed to individual halocarbons. We exclude consideration of diatomic reservoir species (such as HF, HCl and ClO) because although they have relatively high abundances they lack significant mid-infrared absorption features.

$ClONO_2$ has peak mole fractions which can exceed 1 ppb in the extra-tropical mid-stratosphere, resulting primarily from the chlorine released during the degradation of halocarbons (e.g., von Clarmann & Johansson, 2018). The sources of $ClONO_2$ are considered here to follow the fractional contributions to the chlorine component of the mid-latitude equivalent effective stratospheric chlorine (e.g., Newman et al., 2007) (we use the updates to data presented by Hofmann & Montzka (2009) which are available at https://gml.noaa.gov/hats/odgi.html). This data indicates that averaged over the period 2004–2019 (the period covering the satellite data used here, as described in Section 2.2) about 20% of $ClONO_2$ is considered natural in origin (and so excluded from the RF estimates here); 36% of the anthropogenic fraction originates from CFC-11, 24% from CFC-12, 7% from CFC-113, 21% from CCl_4 and 5% from all hydrochlorofluorocarbons (HCFCs). Some of the anthropogenic increase in $ClONO_2$ will originate from nitrous oxide emissions. However, in the period since 1940, during which concentrations of most halocarbons have increased from near zero due to emissions resulting from human activity, nitrous oxide concentrations have increased by only about 15% (e.g., Forster et al., 2021); hence its impact on $ClONO_2$ concentrations is expected to be small.

COF_2 has peak mole fractions which can exceed 0.3 ppb in the tropical upper stratosphere. It is a major degradation product of many CFCs; in terms of abundance, the most important are CFC-12, CFC-113 and HCFC-22 (e.g., Burkholder et al., 2015; Harrison et al., 2014; Prignon et al., 2021).

$COCl_2$ abundance in the stratosphere is mostly controlled by the degradation of CCl_4, with additional contributions from so-called chlorinated very-short-lived substances (VSLSs) (e.g., Bednarz et al., 2022; Harrison et al., 2019; Pettinari et al., 2021). A significant issue with quantifying the RF of $COCl_2$ is disagreement in satellite retrievals of its stratospheric abundance; in different data sets (see Section 2.2) peak mole fractions in the tropical lower stratosphere vary from around 16 ppt (Bernath et al., 2020, 2021) to about 40 ppt (Pettinari et al., 2021).

COClF peaks at about 60 ppt in the tropical lower stratosphere (Bernath et al., 2021; Fu et al., 2009). Its predominant source is degradation of CFC-11 (Burkholder et al., 2015; Fu et al., 2009).

2. Methods

2.1. Radiative Transfer Calculations and Absorption Cross-Sections

Radiative transfer calculations use the 10 cm^{-1} narrow-band model (NBM) described in Shine and Myhre (2020) covering wavenumbers 0–3,000 cm^{-1}, updated to use spectroscopic data for the main greenhouse gases (H_2O, CO_2, O_3, N_2O, CH_4) from the HITRAN2020 database (Gordon et al., 2022). Calculations are performed for mid-season months (January, April, July and October) using zonal-mean atmospheric profiles at 10° latitude resolution, as described in Freckleton et al. (1998) for temperature, water vapor, ozone and cloud amount; the annual-average is taken to be the mean of these four values. Mole-fractions of the well-mixed greenhouse gases are assumed to be their near-contemporary values of 389 ppm for CO_2, 323 ppb for N_2O and 1800 ppb for CH_4. Because of the position of its absorption bands, $ClONO_2$ is most susceptible to overlap with these gases; trial calculations, using 2019 values of the overlapping gases (Forster et al., 2021) altered the $ClONO_2$ RF by ≈0.5%. RF values here are stratosphere-adjusted radiative forcings (SARF) as defined by Forster et al. (2021), in which stratospheric temperatures are adjusted using the standard fixed-dynamical-heating approximation (Fels et al., 1980; Shine & Myhre, 2020); note that wavenumber-integrated SARF is identical at the tropopause and top-of atmosphere (e.g., Shine & Myhre, 2020).

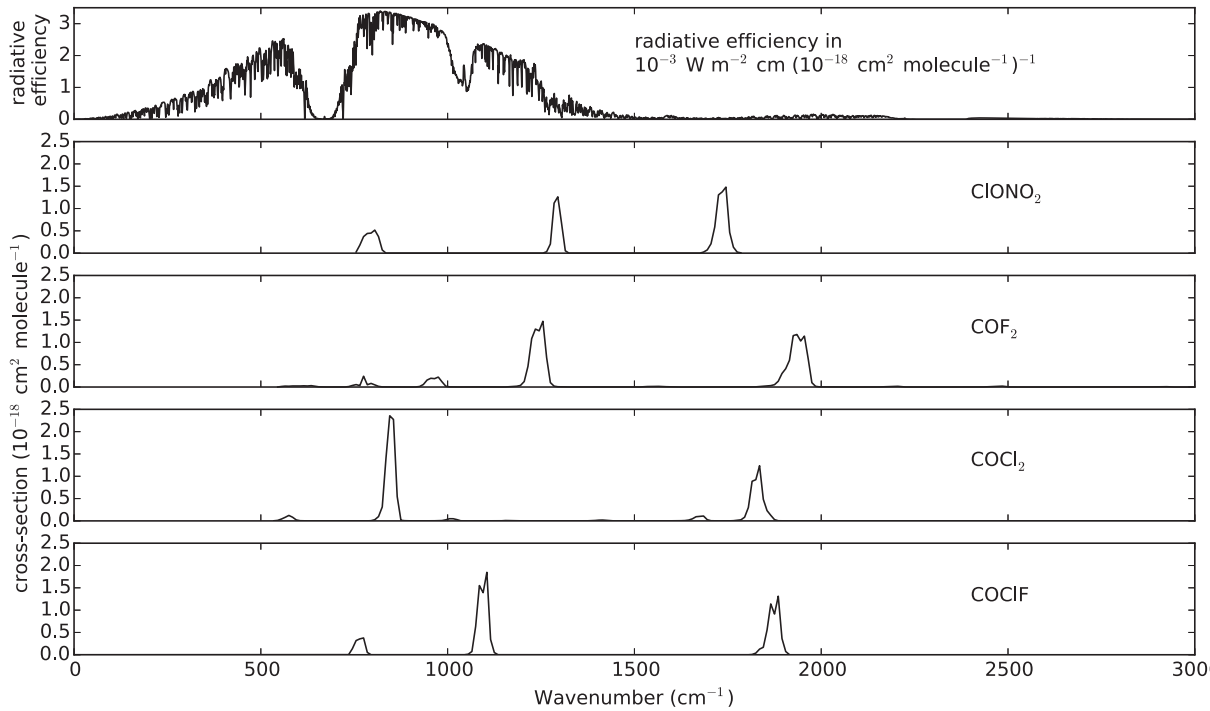

Figure 1. Top Frame: Stratospheric-adjusted radiative efficiency for a well-mixed weak absorber as a function of wavenumber (from Shine & Myhre, 2020); this is presented for illustrative purposes and is not used in the forcing calculations. Subsequent Frames: absorption cross-sections of $ClONO_2$, COF_2, $COCl_2$ and COClF respectively. These are based on existing laboratory measurements at wavenumbers greater than 500 cm^{-1} (see text); any absorption at lower wavenumbers is excluded. Integrated absorption cross-sections are given in Table 1.

Absorption cross-sections at the NBM's 10 cm^{-1} spectral resolution for the target molecules are derived from a variety of sources and shown in Figure 1. For illustration purposes, Figure 1 (top frame) also shows the stratosphere-adjusted spectral radiative efficiency (RE) (the spectral RF per unit change in mole fraction—see Section 3.1) of a well-mixed weak absorber (Shine & Myhre, 2020). This indicates the wavenumbers that contribute most to the spectrally-integrated RE; multiplying this spectral RE by a gas's spectrally-varying absorption cross-section yields, when integrated over wavenumber, that gas's RE. Since the target molecules here have complex horizontal and vertical distributions (see Section 2.2), full NBM calculations are needed, rather than just applying this RE. All available measurements are at wavenumbers greater than about 500 cm^{-1} and thus exclude any RF contributions at lower wavenumbers. Van Hoomissen et al. (2023) present computational evidence that such low wavenumber bands contribute little (normally less than 2%) to the RF of such molecules. Their analysis for two of the molecules presented here ($ClONO_2$ and COF_2) indicates no contribution to the RF from the low wavenumber bands.

$ClONO_2$ absorption cross-sections are taken from HITRAN-2020 (Gordon et al., 2022). For the absorption bands near 780 and 1300 cm^{-1}, the measurements of Wagner and Birk (2003) taken at 249 K are used, as these are closest to typical stratospheric temperatures. For the band near 1700 cm^{-1} the 296 K measurements from Ballard et al. (1988) are used, as only 213 and 296 K measurements are available. The 0–3,000 cm^{-1} integrated absorption cross-section for this choice of data is 1.15×10^{-16} cm^{-1} (molecule cm^{-2})$^{-1}$. Integrated cross-sections for such molecules show little temperature dependence, with a small change in the shape of the absorption band. To illustrate the small effect on RF, sample instantaneous RF calculations were also performed with the 219 K data from Wagner and Birk (2003) and 213 K data from Ballard et al. (1988). The integrated cross-section is only 2.5% lower than the value stated above, which is well within the stated measurement uncertainty. Instantaneous RF values were lower by just 1.8%.

Absorption cross-sections for both COF_2 and $COCl_2$ are derived from 298.15 K measurements from the Pacific Northwest National Laboratory (PNNL) (Sharpe et al., 2004) which cover the spectral region from about 550 to 6,500 cm^{-1} at 0.112 cm^{-1} resolution. These were averaged onto the 10 cm^{-1} NBM grid. COF_2 has several distinct

bands (0–3,000 cm^{-1} integrated cross–section 1.55×10^{-16} cm^{-1} (molecule $cm^{-2})^{-1}$), the strongest of which are away from the peak in spectral RE. By contrast, $COCl_2$ has its strongest band at around 850 cm^{-1}, close to that peak; its 0–3,000 cm^{-1} integrated cross-section is 1.24×10^{-16} cm^{-1} (molecule $cm^{-2})^{-1}$. Although $COCl_2$ line-by-line data is available on HITRAN, this only covers the band centered at 850 cm^{-1}. HITRAN COF_2 line-by-line data covers the four strongest bands shown on Figure 1 but excludes some weaker bands, such as the feature near 600 cm^{-1}. Hence the cross-section data is preferred here.

For COClF, line-by-line data are taken from the GEISA2020 database (Delahaye et al., 2021), which originate from the analysis of measurements by Perrin et al. (2011). This molecule has vibrational bands centered around 760, 1100 and 1900 cm^{-1}. To generate cross-section data, line intensities at 296 K (in cm^{-1} (molecule $cm^{-2})^{-1}$) are summed over the 10 cm^{-1} NBM spectral intervals and then divided by the spectral interval to generate the required cross-sections in cm^2 $molecule^{-1}$. The 0–3,000 cm^{-1} integrated cross-section is 1.18×10^{-16} cm^{-1} (molecule $cm^{-2})^{-1}$.

2.2. Atmospheric Distributions

We base our calculations on trace gas climatologies derived from satellite retrievals from MIPAS (Michelson Interferometer for Passive Atmospheric Sounding e.g., Fischer et al., 2008; Pettinari et al., 2021) and ACE-FTS (Atmospheric Chemistry Experiment Fourier Transform Spectrometer e.g., Bernath et al., 2020, 2021) which provide near-global coverage over a multi-year period. Zonal and annual averages are shown in Figure 2.

For $ClONO_2$, mid-season means are derived from MIPAS data collated for the SPARC (Stratosphere-troposphere Processes And their Role in Climate) Data Initiative (Hegglin et al., 2020; Hegglin et al., 2021; SPARC, 2017) for 2005–2010 (the standard period adopted by SPARC (2017) as a reference for a well-sampled atmosphere). $ClONO_2$ has a significant diurnal variation, which grows in amplitude at pressures less than 10 hPa. MIPAS data is available for 10:00 and 22:00 overpasses. RF calculations are performed for the combined 10:00 and 22:00 data and for each of these separately, to give an indication of the impact of diurnal variation on SARF. The SARF for 22:00 is about 20% higher than that for 10:00; the forcing values presented here are the average of those calculated for the 2 times.

Seasonal-mean climatologies for ACE-FTS (using Version 4.1 retrievals) are presented in Bernath et al. (2021) covering the period 2004–2019. ACE-FTS $ClONO_2$ values are in generally good agreement with MIPAS (SPARC, 2017); however, we assessed the impact on RF of using alternative satellite retrievals by repeating the $ClONO_2$ calculations using ACE-FTS data. For COF_2 and COClF we also use the seasonal-mean ACE-FTS climatologies, as this is the only current source of such climatologies.

For $COCl_2$ there is a significant issue. Between Versions 3.5/3.6 of the ACE-FTS retrieval software (Harrison et al., 2019) and Versions 4.0 (Bernath et al., 2020) and 4.1 (Bernath et al., 2021) the peak mole fractions (in the tropics at about 25 km) fell from ≈40 to ≈15 ppt, a difference that cannot be accounted for by $COCl_2$ trends (about −1 ppt between 2004 and 2020). The earlier ACE-FTS data was generally in good agreement with chemical transport model results (Harrison et al., 2019) and more recent Earth System Model results (Bednarz et al., 2022), indicating that if the later ACE-FTS data is correct, there would be a serious issue in the sources and/or sinks of the modeled $COCl_2$. Pettinari et al. (2021) present MIPAS (v8) retrievals of $COCl_2$ which indicate peaks of ≈40 ppt at around 25 km in the tropics, which are generally in good agreement with the ACE-FTS version 3.5 data (at worst 7 ppt difference) and spectroscopic measurements from a balloon-borne sounder similar to MIPAS. In the absence of a detailed explanation for the difference between earlier and later ACE-FTS results, we tentatively favor the higher values indicated by Harrison et al. (2019) and Pettinari et al. (2021). We present RF results using ACE-FTS version 4.1 and the MIPAS data as presented by Pettinari et al. (2021), where we took the means for the mid-season months across years 2005–2010 for consistency with the MIPAS $ClONO_2$ data as described above.

The MIPAS climatologies were available as monthly and zonal means. The mean for the years 2005–2010 was then taken for the mid-season months January, April, July and October for NBM calculations; the ACE-FTS climatologies from Bernath et al. (2021) are seasonal means covering years 2004–2019.

These climatologies were interpolated onto the NBM climatology levels; the ACE-FTS data was provided using height as the vertical coordinate, whereas the MIPAS data use pressure. The NBM uses both, and interpolation is done using the relevant vertical coordinate from the satellite data. The interpolated concentrations derived from ACE-FTS compare well with the original concentrations as presented in Bernath et al. (2021), confirming that the

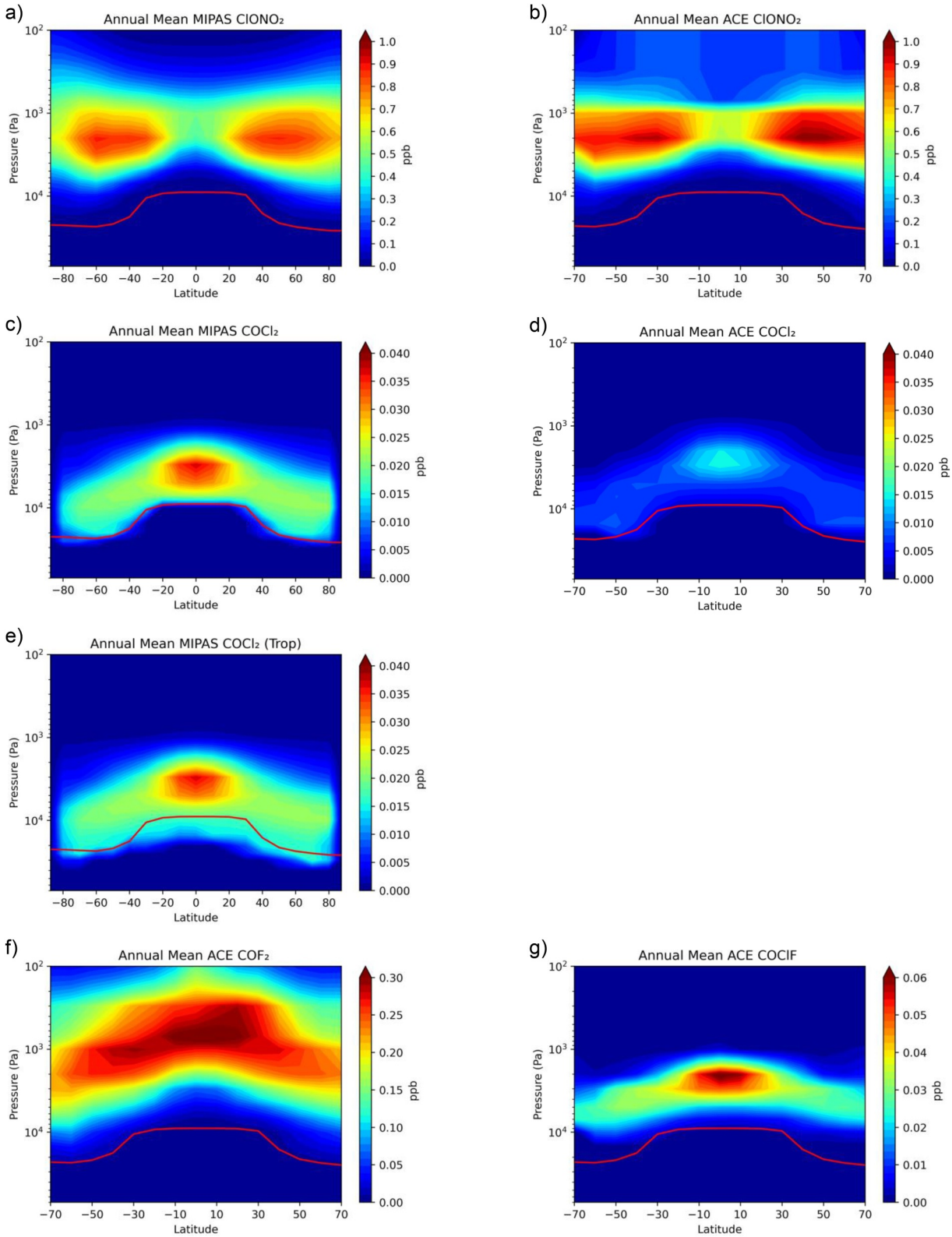

Figure 2. Annual and zonal-mean mole fractions of $ClONO_2$, $COCl_2$, COF_2 and COClF derived from MIPAS and ACE-FTS data interpolated to the grid used for the Narrow Band Model. (a) $ClONO_2$ MIPAS, (b) $ClONO_2$ ACE-FTS, (c) $COCl_2$ MIPAS using a constant tropospheric value of 1 ppt, (d) $COCl_2$ ACE-FTS, (e) $COCl_2$ MIPAS including satellite tropospheric data, (f) COF_2 ACE-FTS, (g) COClF ACE-FTS. The red line indicates the mean tropopause height.

Table 1
Integrated Absorption Cross-Sections (10^{-16} cm^{-1} (molec cm^{-2})$^{-1}$) in the 0–3,000 cm^{-1} Spectral Interval and Stratosphere-Adjusted Radiative Efficiencies (W m^{-2} ppb^{-1}) Assuming the Gases to be Well-Mixed Throughout the Atmosphere

Gas	Integrated absorption cross-sections (10^{-16} cm^{-1} (molec cm^{-2})$^{-1}$) for the 0–3,000 cm^{-1} spectral interval	Radiative efficiency (W m^{-2} ppb^{-1})
$ClONO_2$	1.15	0.092
$COCl_2$	1.24	0.245
COF_2	1.55	0.126
COClF	1.18	0.170

additional processing for use for the NBM retains the original characteristics of the satellite retrievals. In the ACE-FTS data, some high latitude data are not available—poleward of 67.5°S in January, 82.5°S in July and October, and 72.5°N in July; these latitudes are excluded. Averaged over all 4 months, this amounts to ≈2% of the globe, and the impact on the global and annual mean RF will be negligible.

As we are primarily interested in the stratospheric concentrations for these gases, and the satellite data does not generally extend far into the troposphere, a constant value of 0.1 ppt is used below the tropopause for the RF calculations. The same value is used in the cases of missing data. The exception to using this tropospheric value is $COCl_2$, where a value of 1 ppt is used for the tropospheric concentrations based on the model values given in Bednarz et al. (2022), in both the ACE-FTS and MIPAS interpolated data. However, there is a sharp increase in mole fraction in the ACE-FTS data below the tropopause, which was excluded from the interpolation as it seems unlikely to be produced as a breakdown product and may have a different origin or be a spurious artifact in the data retrieval. Similarly, the MIPAS data for $COCl_2$ also shows an extension into the troposphere, but in this case, there is a more gradual transition from stratospheric values, which is anticipated in the modeling studies of Bednarz et al. (2022). For comparison purposes, we use the constant tropopause values for both MIPAS and ACE-FTS data, but we also present the results from the calculation using the MIPAS tropospheric data as it has a noticeable effect on the overall $COCl_2$ RF. Modeling studies indicate that a large proportion of tropospheric $COCl_2$ is likely to be a breakdown product of VSLS origin, with the main parent gases being CH_2Cl_2 and $CHCl_3$ (Bednarz et al., 2022; Hossaini et al., 2015). Figures 2c and 2d show $COCl_2$ ACE-FTS and MIPAS interpolated data with a constant tropopause value, which highlights the differences between these data noted earlier; Figure 2e shows the MIPAS data including tropospheric values.

3. Results

3.1. Radiative Efficiencies

Before discussing RF results, it is useful to present (Table 1) the stratosphere-adjusted RE for the four target molecules assuming them to be well mixed, to illustrate the inherent radiative strength of these molecules. These are annual-global mean results derived using the methods described in Section 2.1. To avoid the possibility of any non-linearity the target molecule is increased from zero to 0.1 ppb; the RE is then presented, following convention (e.g., Hodnebrog et al., 2020), in W m^{-2} ppb^{-1}. For the gases relevant to this study, they remain very close to the linear limit for all mole fractions applied in this paper. For example, for $ClONO_2$, applying a 1 ppb rather than a 0.1 ppb perturbation alters the RE by only 0.4%.

Table 1 confirms that these molecules have high radiative efficiencies; well-mixed values for other halocarbons (e.g., Hodnebrog et al., 2020) are, for example, 0.29 W m^{-2} ppb^{-1} for CFC-11 and 0.18 W m^{-2} ppb^{-1} for HFC-134a. As might be anticipated from Figure 1, $COCl_2$, which has a strong band near 850 cm^{-1}, has the highest RE of the 4 gases considered here; $ClONO_2$, which has its strongest bands beyond about 1200 cm^{-1} where the spectral RE is relatively small, is the weakest.

The only known previously presented REs for some of these gases are in Hodnebrog et al. (2020) (see the Supporting Informationfor that paper). They give a value of 0.086 W m^{-2} $ppb^{-1}$for $ClONO_2$, about 7% lower than the 0.092 W m^{-2} ppb^{-1}found here; this is atleast partly because the strong absorption band near 1700 cm^{-1} was not included in that work. Their value for COF_2 (0.123 W m^{-2} ppb^{-1}) agrees to within 3% of the value given in Table 1. Hodnebrog et al. (2020) did not present RF values using the actual distributions of these gases.

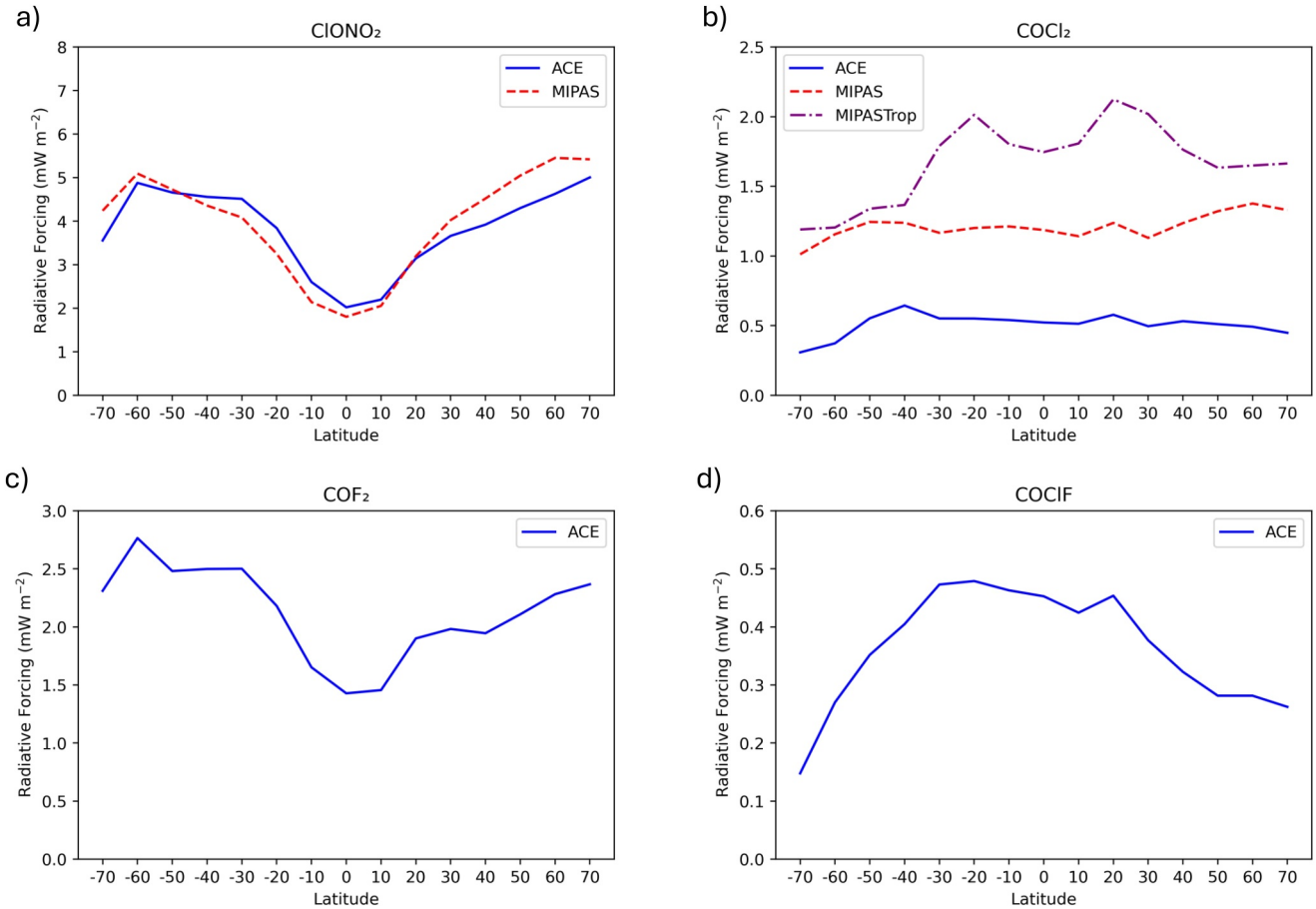

Figure 3. Zonal and annual-mean SARF (in mW m^{-2}) for (a) $ClONO_2$ (b) $COCl_2$ (c) $COCF_2$ (d) COClF.

3.2. Radiative Forcing

Figure 3 presents the zonal and annual-mean SARF for the 4 gases; global and annual-mean forcings are presented in Figure 4. SARF calculations for $ClONO_2$ are reduced by 20% to account for the proportion of $ClONO_2$ which is of natural origin, rather than due to human activity (see Section 1); given the strong linearity in forcing for observed $ClONO_2$ mole fractions discussed in Section 3.1, reducing the SARF, rather than repeating the calculations for the anthropogenic $ClONO_2$ fraction, yields negligible error. The SARF should be considered as representative of the forcing in about 2010 (given the timing of the available satellite climatologies (see Section 2.2)) relative to any preindustrial baseline, recognizing that almost all of it will have occurred since 1940 (Section 1). The detailed time variation of the forcing is not pursued here, as this will depend on the time variation of emissions of different source gases.

The latitudinal variation of SARF is influenced by both the latitudinal and height distribution of the gases. In the case of $ClONO_2$ (Figure 3a), at most latitudes, the peak concentrations are in the mid-stratosphere (Figure 2a) and so the latitudinal variation of SARF is more directly influenced by the magnitude of those peaks; hence SARF is lowest in the tropics, as peak concentrations are lowest there (Figure 2a), and increases by a factor of 2 in the extratropics. Figures 2a and 2b show some differences in the peak concentrations and latitudinal and vertical distribution of $ClONO_2$ between MIPAS and ACE-FTS, but these differences largely compensate when calculating SARF, especially in the global-mean (Figure 4).

For stratospheric $COCl_2$, (Figure 3b), SARF varies relatively little with latitude for both MIPAS and ACE-FTS; the peak concentrations are in the tropical lower-mid stratosphere (Figures 2c and 2d), but this is compensated for by higher concentrations in the extratropical lower stratosphere which, due to density effects, are relatively more important in contributing to the total column. More striking is the factor of more than two difference in SARF (see

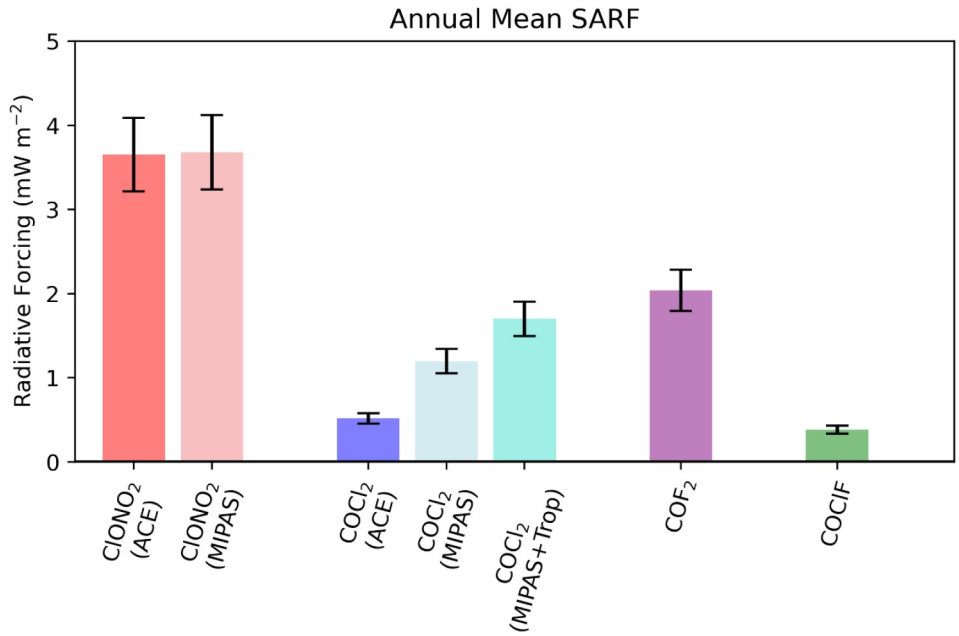

Figure 4. Global and annual mean SARF (in mW m^{-2}). For $ClONO_2$ and $COCl_2$ forcings from both MIPAS and ACE-FTS distributions are provided. For $COCl_2$, an additional value is provided which includes MIPAS $COCl_2$ measurements below the tropopause. The 5%–95% uncertainty range is represented by the error bars.

also Figure 4) which results from the large difference in abundance shown in Figures 2c and 2d. The inclusion of the MIPAS upper tropospheric $COCl_2$ (Figure 2e), which likely originates from chlorine VSLSs (Bednarz et al., 2022), enhances the stratosphere-only SARF by around 50% in the tropics and increases the global-mean value by around 30% (Figure 4).

The latitudinal variation in COF_2 SARF (Figure 3c) is similar to $ClONO_2$ (Figure 3a) but for different reasons; while COF_2 mole fractions peak at about 6 hPa in the tropics, this is more than compensated by the relatively high abundances at higher pressures (and hence densities) in mid-latitudes. By contrast, for COClF (Figure 3d) the extratropical mole fractions are much lower than the peak tropical values, leading to a peak SARF in the tropics.

In terms of global-mean values (Figure 4), $ClONO_2$ is clearly the largest contributor of the gases considered here, giving a SARF of 3.7 mW m^{-2}, followed by COF_2 with 2 mW m^{-2}. The $COCl_2$ contribution is heavily dependent on the choice of ACE-FTS or MIPAS distributions but, given the evidence discussed in Section 2.2, we tentatively favor the MIPAS value, which is 1.2 mW m^{-2}. The COClF contribution is relatively small, around 0.4 mW m^{-2}.

The sum of these is about 7 mW m^{-2}. While clearly this is not a major contributor to total anthropogenic RF, it is nevertheless a systematic positive contribution to the halocarbon RF. Taking values for forcing between 1850 and 2019 from Table 7.5 of Forster et al. (2021), of the 17 halocarbons listed, only 6 have a clearly larger RF (10 mW m^{-2} or greater); these are HFC-134a, CFC-11, CFC-12, CFC-113, HCFC-22 and CCl_4.

It is not straightforward to estimate the uncertainty in these forcings. Hodnebrog et al. (2020) provide an estimate of the 5%–95% confidence range for halocarbon REs, associated with absorption cross-section data, specification of atmospheric profiles and temporal and spatial averaging. These are individually in the range 1%–5%. The dominant uncertainty for short-lived species is in the non-uniform vertical profile, where it is estimated to be about 20%, leading to root-sum-square uncertainty of 24%. Hegglin et al. (2021) discuss sources of uncertainties in satellite retrievals and note that consistent bottom-up estimates are not always available. For $ClONO_2$, which is present in quite high concentrations, the reported standard error near peak concentrations is around ±3%, but it is several times higher for gases present in concentrations typical of the other gases considered here (Figure 2). An additional issue is that spectroscopic uncertainty will affect both retrieval and forcing calculations, and so these are not independent. Any estimated retrieval uncertainties would be unlikely to explain the differences between the MIPAS and ACE-FTS $COCl_2$ mole fractions, which is why we choose to present the RF estimates separately for the two retrievals. We believe that adopting the 5%–95% confidence range of 24% for RE as suggested by

Hodnebrog et al. (2020) will give a conservative estimate of the total uncertainty in the RFs presented here and these are shown in Figure 4. Hence the 90% uncertainty interval for the total forcing is 6.2–7.8 mW m^{-2}.

For individual parent halocarbons, the contribution of the reservoir and breakdown species can be estimated. Appendix A details the fraction of the species that is attributed to five source gases (CFC-11, CFC-12, CFC-113, HCFC-22 and CCl_4) and the consequent enhancement to their forcing. For the first four of these, the increase in their radiative forcings (and radiative efficiencies) is between 0.5% and 3%. CCl_4, which is the major source of stratospheric $COCl_2$ and a contributor to $ClONO_2$, is the major exception. Although a full assessment is limited by the uncertainty in the $COCl_2$ abundance, the stratospheric SARF using MIPAS abundances is around 9% of the CCl_4 direct RF of 13 mW m^{-2} (Forster et al., 2021); this is enhanced by about a further 6% if about 21% of the anthropogenic $ClONO_2$ is attributed to CCl_4, based on its contribution to stratospheric chlorine (see Section 1). Similarly, if about 37% of $ClONO_2$ and all the COClF forcing is attributed to CFC-11, it would enhance the CFC-11 RF by around 3%. The RE and emission metrics such as the Global Warming Potential (GWP) would be impacted by the same amount, since the abundances of the gases considered here are controlled by the lifetime of the parent compound.

Saiz-Lopez et al. (2023) (see their Extended Data Table 5) estimate that the present-day contribution of direct emissions of VSLSs to anthropogenic RF is about −20 mW m^{-2} primarily due to ozone depletion; if all the tropospheric $COCl_2$ RF (about 0.4 mW m^{-2}) was attributed to anthropogenic VSLSs, it would lead to a modest (2%) offset to this forcing.

Stratospheric temperature changes of these gases are a product of the SARF calculations. In all cases, temperature changes, relative to a zero background for each gas, are minor, the highest being a 0.14 K cooling due to $ClONO_2$.

4. Conclusions

We are aware of no previous study that has quantified the RF due to polyatomic reservoir and breakdown products of halocarbon source gases. Some of these gases have both high concentrations in the stratosphere, relative to the source gases and, as has been demonstrated here, when well-mixed, the four target compounds have high radiative efficiencies, again compared to their source gases.

Employing recent satellite-derived climatologies of their stratospheric distribution, we have presented the first calculations of the RF for $ClONO_2$, $COCl_2$, COF_2 and COClF. Collectively, the estimated forcing is about 7 mW m^{-2}, relative to a pre-industrial baseline, almost all of it occurring since 1940, with a 90% uncertainty interval of 6.2–7.8 mW m^{-2}. This uncertainty interval does not include the uncertainty in $COCl_2$ forcing arising from the disagreement between recent satellite-derived concentrations of the gas yield forcings that disagree by about a factor of three; had retrievals from ACE-FTS Version 3.6 been used rather than Version 4.1, the agreement with MIPAS would have been much better.

Hence, this work indicates that these 4 gases lead to a small systematic increase in direct halocarbon RF (estimated to be 0.41 W m^{-2} for the period 1850–2019—see Section 1). Nevertheless, only six individual halocarbons have a forcing greater than that calculated here. For CCl_4, a major source of $COCl_2$ and a minor source of $ClONO_2$, its direct forcing (taking the higher of the two satellite concentrations of $COCl_2$ used here) and hence GWP, is estimated to be enhanced by about 15% because of these contributions. This is significant as although direct use of CCl_4 (e.g., as a solvent) is no longer allowed under the terms of the Montreal Protocol, it is widely used as a feedstock input for hydrofluorocarbon and hydrofluoroolefin production; production of CCl_4 is increasing (Figures 7–3 of WMO (2022)) and, possibly as a result, inferred emissions have remained approximately constant in the past decade, following the rapid decline from peak emissions in the early 1990s (Figures 1–3 of WMO (2022)).

A further context is that the total halocarbon RF should include indirect effects (principally on ozone, but also on methane, aerosol-cloud and aerosol-radiation interactions), of which the work presented here is an additional contributor and the only one that has been identified to give a positive contribution. Szopa et al. (2021) (Figure 6.12) show that the best estimate of the total halocarbon effective RF (ERF) for the period 1750–2019 is approximately 0.21 W m^{-2} and so about half that of the direct halocarbon ERF, with high uncertainty (the 5%–95% range of the total ERF being 0.02–0.40 W m^{-2}); thus, the gases considered here could enhance the central estimate of the total halocarbon RF by around 3.3% (or between 1.7% and 35% for the 5%–95% uncertainty range).

On an individual gas basis, the GWP and other metrics for emissions of halocarbons are impacted by these indirect effects, especially the ozone-depleting substances (ODSs). WMO (2022) Section 7.3.2 presents estimated 100-year GWP values for both the direct and indirect effects. For several chlorinated ODSs, notably CFC-11, CFC-12 and CFC-113, the indirect GWP offsets more than 25% of the direct GWP, and in the case of CCl_4 it exceeds the direct GWP. Taking these estimates at face value, the net CCl_4 GWP given by WMO (2022) (−1,310) would change by nearly 20% to −1,095 if the higher value of $COCl_2$ forcing calculated here (using MIPAS retrievals) is used.

Based on both the observed concentrations of these gases, and their known spectroscopic properties, we believe we have isolated the major contributors to RF from such halocarbon reservoir and breakdown products; however, other such species will undoubtedly contribute further RF and could be worthy of future investigation. Further, the time variation of these forcings will depend on the detailed time variation of the source gases, their rate of breakdown, and the effect of changes in the stratospheric circulation (e.g., Fu et al., 2019) on their distribution, which could also be pursued in further work.

Appendix A: Approximate Attribution of Halogen Reservoir and Halocarbon Breakdown Products to Source Gas

Approximate contributions of source gases to the increased abundances of each of the 4 gases considered here are given in Table A1. Direct RFs are from Table 7.5 of Forster et al. (2021) for the period of 1850–2019 although this forcing is predominantly after 1940. $ClONO_2$ fractions are derived using effective equivalent stratospheric chlorine as described in Section 1 and exclude the natural background concentrations of $ClONO_2$. Approximate COF_2 fractions are derived from tropical mid-stratospheric loss rates of CFC-11, CFC-113 and HCFC-22 from model calculations in Harrison et al. (2014) (their Figure 10). CCl_4 is assumed the dominant source of stratospheric $COCl_2$ following Harrison et al. (2019) and CFC-11 is assumed the dominant source of COClF following Fu et al. (2009) and Burkholder et al. (2015).

Table A1

Approximate Attribution of the Forcing (Shown in Parentheses) Due To $ClONO_2$, COF_2, $COCl_2$ and COClF to Individual Source Gases, as Described in the Text. The Second Column Gives the Direct Forcing of the Source Gas. The Fraction of Total Forcing (Which is Shown in Parentheses) Due To Each Reservoir/Breakdown Species is Given in the Next Four Columns. The Final Column Then Shows the Percentage Total Enhancement of the Direct Forcing Due To the 4 Reservoir/Breakdown Species. The MIPAS Stratospheric $COCl_2$ Forcing is Used Here

		Approximate fraction of reservoir/breakdown forcing attributed to each source gas (RF in mW m^{-2} due to each gas is shown in parentheses)				
	Direct RF (mW m^{-2})	$ClONO_2$ (3.7)	COF_2 (2)	$COCl_2$ (1.2)	COClF (0.4)	Percentage increase in direct forcing due to all reservoir species/breakdown products
CFC-11	66	0.36	–	–	1	2.6
CFC-12	180	0.26	0.86	–	–	1.5
CFC-113	21	0.07	0.11	–	–	2.3
HCFC-22	53	0.05	0.03	–	–	0.5
CCl_4	13	0.21		1	–	15.3

Data Availability Statement

All SPARC Data Initiative zonal monthly mean data sets can be found in the Zenodo data archive (Hegglin et al., 2020, https://doi.org/10.5281/zenodo.4265392). ACE-FTS climatologies are available in the Supplementary Materials of Bernath et al. (2021). $ClONO_2$ absorption cross-sections are available on the HITRAN database https://hitran.org/. PNNL $COCl_2$ absorption cross-sections are available in the HITRAN database supplemental folder https://hitran.org/suppl/xsec/. COClF line-by-line data is available on the GEISA database https://geisa.aeris-data.fr/. These absorption cross-sections averaged at 10 cm^{-1} spectral resolution are included in a .csv file in the Supporting Information (Table S1).

Acknowledgments
The work originated from a suggestion by Øivind Hodnebrog. It was funded by the UK Natural Environment Research Council Grant "Investigating Halocarbon Impacts on the global environment" (Grant Reference NE/X004198/1) led by the University of Bristol, UK. Martyn Chipperfield, Michaela Hegglin, Ryan Hossaini and two reviewers provided helpful comments on earlier versions. Damien Weidmann is thanked for help in accessing spectroscopic data. Paolo Pettinari provided phosgene climatologies retrieved from MIPAS observations.

References

Ballard, J., Johnston, W. B., Gunson, M. R., & Wassell, P. T. (1988). Absolute absorption coefficients of $ClONO_2$ infrared bands at stratospheric temperatures. *Journal of Geophysical Research*, *93*(D2), 1659–1665. https://doi.org/10.1029/JD093iD02p01659

Bednarz, E. M., Hossaini, R., Chipperfield, M. P., Abraham, N. L., & Braesicke, P. (2022). Atmospheric impacts of chlorinated very short-lived substances over the recent past – Part 1: Stratospheric chlorine budget and the role of transport. *Atmospheric Chemistry and Physics*, *22*(16), 10657–10676. https://doi.org/10.5194/acp-22-10657-2022

Bernath, P. F., Crouse, J., Hughes, R. C., & Boone, C. D. (2021). The Atmospheric Chemistry Experiment Fourier transform spectrometer (ACE-FTS) version 4.1 retrievals: Trends and seasonal distributions. *Journal of Quantitative Spectroscopy and Radiative Transfer*, *259*, 107409. https://doi.org/10.1016/j.jqsrt.2020.107409

Bernath, P. F., Steffen, J., Crouse, J., & Boone, C. D. (2020). Sixteen-year trends in atmospheric trace gases from orbit. *Journal of Quantitative Spectroscopy and Radiative Transfer*, *253*, 107178. https://doi.org/10.1016/j.jqsrt.2020.107178

Burkholder, J. B., Cox, R. A., & Ravishankara, A. R. (2015). Atmospheric degradation of ozone depleting substances, their substitutes, and related species. *Chemical Reviews*, *115*(10), 3704–3759. https://doi.org/10.1021/cr5006759

Delahaye, T., Armante, R., Scott, N. A., Jacquinet-Husson, N., Chédin, A., Crépeau, L., et al. (2021). The 2020 edition of the GEISA spectroscopic database. *Journal of Molecular Spectroscopy*, *380*, 111510. https://doi.org/10.1016/j.jms.2021.111510

Fels, S. B., Mahlman, J. D., Schwarzkopf, M. D., & Sinclair, R. W. (1980). Stratospheric sensitivity to perturbations in ozone and carbon dioxide: Radiative and dynamical response. *Journal of the Atmospheric Sciences*, *37*(10), 2265–2297. https://doi.org/10.1175/1520-0469(1980)037<2265:SSTPIO>2.0.CO;2

Fischer, H., Birk, M., Blom, C., Carli, B., Carlotti, M., von Clarmann, T., et al. (2008). MIPAS: An instrument for atmospheric and climate research. *Atmospheric Chemistry and Physics*, *8*, 2151–2188. https://doi.org/10.5194/acp-8-2151-2008

Forster, P., Storelvmo, T., Armour, K., Collins, W., Dufresne, J.-L., Frame, D., et al. (2021). The Earth's energy budget, climate feedbacks, and climate sensitivity. In V. Masson-Delmotte et.al. (Eds.), *Climate change 2021: The physical science basis. Contribution of working group I to the sixth assessment report of the intergovernmental Panel on climate change* (pp. 923–1054). Cambridge University Press. https://doi.org/10.1017/9781009157896.009

Freckleton, R., Highwood, E., Shine, K., Wild, O., Law, K., & Sanderson, M. (1998). Greenhouse gas radiative forcing: Effects of averaging and inhomogeneities in trace gas distribution. *Quarterly Journal of the Royal Meteorological Society*, *124*(550), 2099–2127. https://doi.org/10.1256/smsqj.55013

Fu, D., Boone, C. D., Bernath, P. F., Weisenstein, D. K., Rinsland, C. P., Manney, G. L., & Walker, K. A. (2009). First global observations of atmospheric COClF from the atmospheric chemistry experiment mission. *Journal of Quantitative Spectroscopy and Radiative Transfer*, *110*(12), 974–985. https://doi.org/10.1016/j.jqsrt.2009.02.018

Fu, Q., Solomon, S., Pahlavan, H. A., & Lin, P. (2019). Observed changes in Brewer–Dobson circulation for 1980–2018. *Environmental Research Letters*, *14*(11), 114026. https://doi.org/10.1088/1748-9326/ab4de7

Gordon, I. E., Rothman, L. S., Hargreaves, R. J., Hashemi, R., Karlovets, E., Skinner, F., et al. (2022). The HITRAN2020 molecular spectroscopic database. *Journal of Quantitative Spectroscopy and Radiative Transfer*, *277*, 107949. https://doi.org/10.1016/j.jqsrt.2021.107949

Harrison, J. J., Chipperfield, M. P., Dudhia, A., Cai, S., Dhomse, S., Boone, C. D., & Bernath, P. F. (2014). Satellite observations of stratospheric carbonyl fluoride. *Atmospheric Chemistry and Physics*, *14*(21), 11915–11933. https://doi.org/10.5194/acp-14-11915-2014

Harrison, J. J., Chipperfield, M. P., Hossaini, R., Boone, C. D., Dhomse, S., Feng, W., & Bernath, P. F. (2019). Phosgene in the upper troposphere and lower stratosphere: A marker for product gas injection due to chlorine-containing very short-lived substances. *Geophysical Research Letters*, *46*(2), 1032–1039. https://doi.org/10.1029/2018GL079784

Hegglin, M. I., Tegtmeier, S., Anderson, J., Bourassa, A. E., Brohede, S., Degenstein, D., et al. (2020). SPARC Data Initiative monthly zonal mean composition measurements from stratospheric limb sounders (1978-2018) (Version p01) [Dataset]. *Earth System Science Data, Zenodo*. https://doi.org/10.5281/zenodo.4265392

Hegglin, M. I., Tegtmeier, S., Anderson, J., Bourassa, A. E., Brohede, S., Degenstein, D., et al. (2021). Overview and update of the SPARC data initiative: Comparison of stratospheric composition measurements from satellite limb sounders. *Earth System Science Data*, *13*(5), 1855–1903. https://doi.org/10.5194/essd-13-1855-2021

Hodnebrog, Ø., Aamaas, B., Fuglestvedt, J. S., Marston, G., Myhre, G., Nielsen, C. J., et al. (2020). Updated global warming potentials and radiative efficiencies of halocarbons and other weak atmospheric absorbers. *Reviews of Geophysics*, *58*(3), e2019RG000691. https://doi.org/10.1029/2019RG000691

Hofmann, D. J., & Montzka, S. A. (2009). Recovery of the ozone layer: The ozone depleting gas index. *Eos, Transactions American Geophysical Union*, *90*(1), 1–2. https://doi.org/10.1029/2009EO010001

Hossaini, R., Chipperfield, M. P., Saiz-Lopez, A., Harrison, J. J., von Glasow, R., Sommariva, R., et al. (2015). Growth in stratospheric chlorine from short-lived chemicals not controlled by the Montreal Protocol. *Geophysical Research Letters*, *42*(11), 4573–4580. https://doi.org/10.1002/2015GL063783

Newman, P. A., Daniel, J. S., Waugh, D. W., & Nash, E. R. (2007). A new formulation of equivalent effective stratospheric chlorine (EESC). *Atmospheric Chemistry and Physics*, *7*, 4537–4552. https://doi.org/10.5194/acp-7-4537-2007

Perrin, A., Demaison, J., & Toon, G. (2011). The ν_1, ν_2, and ν_3 bands of carbonyl chlorofluoride (COFCl) at 5.3, 9.1, and 13.1 μm: Position and intensity parameters and their use for atmospheric studies. *Journal of Quantitative Spectroscopy and Radiative Transfer*, *112*(8), 1266–1279. https://doi.org/10.1016/j.jqsrt.2011.01.003

Pettinari, P., Barbara, F., Ceccherini, S., Dinelli, B. M., Gai, M., Raspollini, P., et al. (2021). Phosgene distribution derived from MIPAS ESA v8 data: Intercomparisons and trends. *Atmospheric Measurement Techniques*, *14*(12), 7959–7974. https://doi.org/10.5194/amt-14-7959-2021

Prignon, M., Chabrillat, S., Friedrich, M., Smale, D., Strahan, S. E., Bernath, P. F., et al. (2021). Stratospheric fluorine as a tracer of circulation changes: Comparison between infrared remote-sensing observations and simulations with five modern reanalyses. *Journal of Geophysical Research: Atmospheres*, *126*(19), e2021JD034995. https://doi.org/10.1029/2021JD034995

Saiz-Lopez, A., Fernandez, R. P., Li, Q., Cuevas, C. E., Fu, X., Kinnison, D. E., et al. (2023). Natural short-lived halogens exert an indirect cooling effect on climate. *Nature*, *618*(7967), 967–973. https://doi.org/10.1038/s41586-023-06119-z

Sharpe, S. W., Johnson, T. J., Sams, R. L., Chu, P. M., Rhoderick, G. C., & Johnson, P. A. (2004). Gas-phase databases for quantitative infrared spectroscopy. *Applied Spectroscopy*, *58*(12), 1452–1461. https://doi.org/10.1366/0003702042641281

Shine, K. P., & Myhre, G. (2020). The spectral nature of stratospheric temperature adjustment and its application to halocarbon radiative forcing. *Journal of Advances in Modeling Earth Systems*, *12*(3), e2019MS001951. https://doi.org/10.1029/2019MS001951

SPARC. (2017). The SPARC Data Initiative: Assessment of stratospheric trace gas and aerosol climatologies from satellite limb sounders. In M. I. Hegglin & S. Tegtmeier (Eds.), *SPARC report No. 8, WCRP-5/2017*. https://doi.org/10.3929/ethz-a-010863911

Szopa, S., Naik, V., Adhikary, B., Artaxo, P., Berntsen, T., Collins, W. D., et al. (2021). Short-lived climate forcers. In V. Masson-Delmotte et al. (Eds.), *Climate change 2021: The physical science basis. Contribution of working group I to the sixth assessment report of the intergovernmental Panel on climate change* (pp. 817–922). Cambridge University Press. https://doi.org/10.1017/9781009157896.008

Van Hoomissen, D., Papadimitriou, V. C., & Burkholder, J. B. (2023). Low frequency (<500 cm^{-1}) contribution to greenhouse gas radiative efficiency. *Molecular Physics*, *122*(7–8). e2273412. https://doi.org/10.1080/00268976.2023.2273412

von Clarmann, T., & Johansson, S. (2018). Chlorine nitrate in the atmosphere. *Atmospheric Chemistry and Physics*, *18*(20), 15363–15386. https://doi.org/10.5194/acp-18-15363-2018

Wagner, G., & Birk, M. (2003). New infrared spectroscopic database for chlorine nitrate. *Journal of Quantitative Spectroscopy and Radiative Transfer*, *82*(1–4), 443–460. https://doi.org/10.1016/S0022-4073(03)00169-9

WMO. (2022). *Scientific assessment of ozone depletion: 2022, GAW report No. 278* (p. 509). World Meteorological Organization. Retrieved from https://ozone.unep.org/system/files/documents/Scientific-Assessment-of-Ozone-Depletion-2022.pdf